Aromatic and Methyl NOEs Highlight Hydrophobic Clustering in the Unfolded State of an SH3 Domain†

Karin A. Crowhurst‡,§ and Julie D. Forman-Kay*,‡,§

Structural Biology and Biochemistry Program, Hospital for Sick Children, Toronto, Ontario, M5G 1X8 Canada, and Department of Biochemistry, University of Toronto, Toronto, Ontario, M5S 1A1 Canada

Received April 14, 2003; Revised Manuscript Received May 21, 2003

ABSTRACT: The N-terminal SH3 domain of *Drosophila* drk (drkN SH3 domain) exists in equilibrium between a folded (F_{exch}) state and a relatively compact unfolded (U_{exch}) state under nondenaturing conditions. Selectively labeled samples of the domain have been analyzed by NOESY NMR experiments to probe residual hydrophobic clustering in the U_{exch} state. The labeling strategy included selective protonation of aromatic rings or δ-methyl groups on Ile and Leu residues in a highly deuterated background. Combined with long mixing times, the methods permitted observation of significant numbers of long-range interactions between hydrophobic side chains, providing evidence for multiple conformers involving non-native hydrophobic clusters around the Trp 36 indole. Comparison of these data with previously reported HN−HN NOEs yields structural insight into the diversity of structures within the U_{exch} ensemble in the drkN SH3 domain. Many of the HN−HN NOEs are consistent with models containing compact residual nativelike secondary structure and greater exposure of the Trp 36 indole to solvent, similar to kinetic intermediates formed in the hierarchic condensation model of folding. However, the methyl and aromatic NOE data better fit conformations with non-native burial of the Trp indole surrounded by hydrophobic groups and more loosely formed β-structure; these structural characteristics are more consistent with those of kinetic intermediates formed during the hydrophobic collapse mechanism of folding. This suite of NOE data provides a more complete picture of the structures that span the U_{exch} state ensemble, from conformers with non-native structure but long-range contacts to those that are highly nativelike. Together, the results are also consistent with the folding funnel view involving multiple folding pathways for this molecule.

An understanding of the mechanisms of protein folding and the factors influencing protein stability has been a goal for many researchers. While the importance of hydrogen bonds and electrostatic contacts is still debated, there is mounting evidence that hydrophobic interactions play significant roles in driving protein folding, as well as in stabilizing compact disordered states (*1*−*4*). A number of recent studies suggest that hydrophobic groups mediate long-range contacts in disordered proteins (*2*, *5*−*7*). In some cases, residual structure in unfolded states has been described as long-range, dynamic hydrophobic clustering interactions (*8*). This contrasts with reports of residual turns, nascent helices, or strands, suggesting that secondary structure forms on a kinetic path to the folded state (*9*, *10*).

One example of stabilized hydrophobic interactions in a disordered state is in the unfolded state of lysozyme, which has been probed using NMR[1] and site-directed mutagenesis (*2*). Analysis of chemical shift changes and ^{15}N transverse relaxation rate experiments indicated that the largest clusters of residual structure involved hydrophobic groups, especially the six Trp residues in the molecule. Interestingly, the crucial stabilizing role played by Trp 62 highlights the value of non-native hydrophobic interactions in the unfolded state in preventing proteins from aggregating instead of folding. In another study of chemical shifts and *J*-coupling data in acid-unfolded apomyoglobin (*5*), it was observed that the restriction in backbone fluctuations of residues 28−34 was more likely due to hydrophobic collapse than nativelike helical contacts or other transient secondary structure. Fluorescence and NMR peak intensity experiments on intestinal fatty acid binding protein (IFABP) in varying concentrations of urea suggested that persistent structure in the initial steps of folding is comprised of hydrophobic clusters of Val, Leu, Tyr, Phe, and Ile (*6*). NMR experiments performed on papillomavirus E2 DNA binding domain in 3 M urea also highlighted three sequential hydrophobic residues that show evidence for a stabilized structure (*7*).

While these studies demonstrate the presence of long-range hydrophobic interactions, few medium- and long-range NOEs

† This work was supported by a grant to J.D.F.-K. from the Canadian Institutes of Health Research (CIHR). K.A.C. acknowledges the CIHR for a Doctoral Research Award.

* To whom correspondence should be addressed. Phone: (416) 813-5358. Fax: (416) 813-5022. E-mail: forman@sickkids.ca.

‡ University of Toronto.

§ Hospital for Sick Children.

[1] Abbreviations: SH3, Src homology 3 domain; drkN SH3, N-terminal SH3 domain of *Drosophila* drk; U_{exch} and F_{exch}, the unfolded and folded state of the drkN SH3 domain; SAXS, small-angle X-ray scattering; R_g, radius of gyration; NMR, nuclear magnetic resonance; HSQC, heteronuclear single quantum coherence; NOE, nuclear Overhauser effect; NOESY, NOE spectroscopy; exchange NOE, exchange between F_{exch} and U_{exch} states takes place during NOE transfer; TOCSY, total correlation spectroscopy; FID, free induction decay; TRADES, trajectory directed ensemble sampling; DSS, 2,2-dimethyl-2-silapentane-5-sulfonate; M9, minimal media.

10.1021/bi034601p CCC: $25.00
Published on Web 07/03/2003

($i, \geq i + 4$) have been observed in unfolded states of proteins using standard parameters and NMR techniques (*11*, *12*). In some cases, this is due to the extended, almost random coil-like structure in highly denatured proteins. In ensembles of unfolded states that have been studied under more weakly denaturing conditions and show evidence for higher populations of more compact conformations, medium- and long-range interactions may not be seen in standard NMR samples because NOE peaks are too weak to be seen above the spectral noise. Their weakness is due to the transient nature of these interactions, with medium- or long-range contacts only existing within a subset of molecules in the ensemble. Full or selective deuteration of the sample can be employed to combat this problem. The elimination of relaxation pathways in both ^{1}H and ^{13}C dimensions leads to decreased line widths and an enhanced signal-to-noise ratio, facilitating observation of weaker peaks that would otherwise be obscured (*13*). The decrease in spin diffusion pathways also permits increased mixing times from typical values of 100−200 ms for protonated systems to 500−600 ms in deuterated samples (*14*, *15*). This is particularly important for successful detection of long-range distance restraints (*13*, *15*, *16*). Selective protonation permits retention of particular sets of protons in an otherwise fully deuterated background; only NOEs between selected functional groups or residues are observed, with decreased overlap and with improvement of relaxation properties. If deuteration is combined with selective ^{1}H- and ^{13}C-,^{15}N-labeling, NOEs can be recorded and resolved. One disadvantage of these labeling methods, of course, is the decrease in the number of protons available for recording NOEs, resulting in fewer distance restraints or the requirement to prepare several selectively labeled samples to obtain a variety of NOE restraints. However, in the study of disordered proteins the benefits are substantial.

The N-terminal SH3 domain of *Drosophila* drk (drkN SH3), which exists in equilibrium under nondenaturing conditions between a folded (F_{exch}) and highly populated unfolded (U_{exch}) state, has been extensively studied by our group (*11*, *12*, *17*−*23*). SAXS (small-angle X-ray scattering) and NMR diffusion experiments have demonstrated that the radius of gyration and hydrodynamic radius, respectively, of the unfolded state are intermediate between that of the folded state and a random coil structure (*24*). Since it is quite compact, some conformers in this U_{exch} ensemble might resemble kinetic intermediates formed during the first stage of protein folding proposed by the hydrophobic collapse mechanism (*25*), where the protein forms a more compact state with long-range interactions but no regular secondary structure. Stopped-flow fluorescence, near-UV circular dichroism, and hydrogen-exchange NMR experiments have provided evidence that the single Trp 36 indole has, on average, greater burial in the U_{exch} than the F_{exch} state (*17*, *25*), which may be explained by involvement in non-native hydrophobic clustering. Consequently, we decided that targeted investigation of residual hydrophobic interactions could provide valuable structural information about the unfolded state ensemble. Here, we describe the results of experiments measuring NOEs involving methyl-containing as well as aromatic residues using selectively labeled protein samples. We also compare these data with previously reported HN−HN NOEs (*26*) to gain a comprehensive picture of both hydrophobic clustering as well as residual secondary structure maintained in the unfolded state of the drkN SH3 domain.

EXPERIMENTAL PROCEDURES

Sample Preparation. The ^{15}N,^{13}C,^{2}H methyl protonated (Leu $C^{\delta 1/\delta 2}$ and Ile C^{δ}) drkN SH3 domain sample was prepared using ^{13}C,^{2}H glucose and $^{15}N^{2}H_4Cl$ as carbon and nitrogen sources, respectively, supplemented by the precursors [3-^{2}H] ^{13}C α-ketoisovalerate and [3,3 $^{2}H_2$] ^{13}C α-ketobutyrate, generated from ^{15}N,^{13}C L-threonine as described previously (*14*, *27*). The sample was prepared using modifications to a deuteration protocol outlined by Mok et al. (*25*). A single colony of *Escherichia coli* BL21 (DE3) carrying the drkN SH3 domain plasmid (*22*) was inoculated into a 200 mL solution of LB and carbenicillin (100 mg mL^{-1}) in a 1 L flask and shaken slowly (150 rpm) at 25 °C overnight (∼13.5 h). This culture was centrifuged (4000 rpm, 30 °C, 5 min), and a portion of the pellet was resuspended into 50 mL of $^{15}NH_4Cl/^{1}H_2O/^{1}H$,^{12}C-glucose M9 medium in a 250 mL flask to obtain a starting A_{600} of approximately 0.1. This was shaken (250 rpm, 37 °C) until A_{600} ∼0.6, at which time 15 mL of the culture was centrifuged (6000 rpm, 37 °C, 5 min). The pellet was resuspended into 100 mL of $^{15}NH_4Cl/^{2}H_2O/^{1}H$,^{12}C-glucose M9 medium in a 500 mL flask (again, starting A_{600} ∼0.1) and shaken until A_{600} ∼0.4. A total of 100 mL of this culture was pelleted and resuspended into 400 mL of $^{15}N^{2}H_4Cl/^{2}H_2O/^{2}H$,^{12}C-glucose M9 medium in a 2 L flask (starting A_{600} ∼0.1). The solution was shaken until A_{600} ∼0.5, and sufficient culture was pelleted to obtain a starting A_{600} ∼0.1 when resuspended into 2 × 750 mL of $^{15}N^{2}H_4Cl/^{2}H_2O/^{2}H$,^{12}C-glucose M9 medium in 2.8 L fernbach flasks. The solutions were shaken until 1 h before induction, at which time 250 mL of the precursor mixture was added to each flask, resulting in concentrations of 50 and 100 mg L^{-1} for [3,3 $^{2}H_2$] ^{13}C α-ketobutyrate and [3-^{2}H] ^{13}C α-ketoisovalerate, respectively. Protein expression was induced at A_{600} ∼0.7 by adding IPTG (250 mg/L of culture), and the culture was grown for three more hours before harvesting. The cells were lysed using a combination of 0.5 mg mL^{-1} lysozyme and 1.2 mg mL^{-1} deoxycholic acid in buffer A (50 mM Tris, 2 mM EDTA, and 5 mM benzamidine, pH 7.5) and sonication. All purification steps were performed at 4 °C. Purification of the sample differed slightly from the standard protocol for the drkN SH3 domain (*23*, *25*): after elution from a DE-52 anion-exchange column and one round of purification under standard buffer conditions on a Superdex 75 gel-filtration column, it was necessary to perform a second round on the Superdex 75 column using 4 M guanidinium chloride in the buffer to separate out residual impurities. A yield of approximately 10 mg/L growth was obtained.

The drkN SH3 domain sample used for aromatic NOE experiments was fully ^{15}N,^{12}C,^{2}H-labeled, except for fully ^{15}N,^{13}C,^{1}H-labeled Trp, Tyr, Phe, and His residues. For the purposes of these experiments, His was included with the aromatic residues. The growth protocol was similar to the above outline, except that a different precursor solution was added 1 h before induction. Once mixed, each fernbach contained 1 L of $^{15}N^{2}H_4Cl/^{2}H_2O/^{2}H$,^{12}C-glucose M9 medium with 75 mg L^{-1} free $^{15}N/^{1}H/^{13}$C L-Trp, L-Tyr, and L-Phe amino acids, as well as 100 mg L^{-1} $^{15}N/^{1}H/^{13}$C L-His·HCl·H_2O. Cell lysis was performed as described above. All

purification steps were performed at 4 °C. The protein was first purified on a DE-52 anion exchange column with a linear gradient of NaCl (0−1.0 M), then on a Superdex 75 gel-filtration column using a Pharmacia FPLC system. In the final purification step, the sample was dialyzed into 0.4 M Na_2SO_4 in buffer A (see above) and loaded onto a Mono S cation exchange column. The pure sample eluted while the column was washed with 0 M salt buffer. A yield of approximately 7 mg/L growth was obtained. All isotopically labeled reagents were purchased from Cambridge Isotope Labs.

HN−HN NOE Experiment. All NMR data were processed using NMRPipe/NMRDraw (*28*, *29*) and analyzed with NMRView (*30*, *31*) software on a Linux-based PC. Assignment of backbone amide resonances has been reported previously (*32*), but a 3-D HNCα$C\beta$ spectrum (*33*) was recorded on a Varian UNITY 500 MHz spectrometer at 5 °C to assign backbone NH_2 resonances from Asn, Gln, and Arg that are also seen in the amide regions of NOESY experiments. A ^{13}C,^{15}N-labeled, 2.2 mM sample of the drkN SH3 domain in sodium phosphate (50 mM, pH 6) with 10% D_2O and 200 μM DSS (2,2-dimethyl-2-sila-pentane-5-sulfonate) was used.

A 3-D HSQC−NOESY−HSQC experiment (*23*) was recorded at 5 °C on a 1.5 mM ^{15}N,^{13}C,^{2}H-labeled, δ-methyl ^{1}H-labeled drkN SH3 sample in sodium phosphate (50 mM, pH 6), 10% D_2O, and 200 μM DSS recorded on a Varian Inova 800 MHz spectrometer equipped with pulsed-field gradient triple resonance probes. A 600 ms mixing time and 64 ms acquisition time were utilized. Details of experimental parameters and processing have been described elsewhere (*26*).

Methyl NOE NMR Experiments. Experiments were recorded at 5 °C on a 1.5 mM ^{15}N,^{13}C,^{2}H-labeled, δ-methyl ^{1}H-labeled drkN SH3 sample in sodium phosphate (50 mM, pH 6), 10% D_2O, and 200 μM DSS. Experiments to assign methyl resonances were recorded on a Varian Inova 800 MHz spectrometer equipped with a pulsed-field gradient triple resonance probe. The 3-D CCC−TOCSY−NNH experiment (*34*) utilized a matrix of 42 × 32 × 768 complex points and spectral widths of 4000.0, 1783.0, and 12001.2 Hz for F_1, F_2, and F_3, respectively. The constant time ^{13}C-^{1}H HSQC (*35*) utilized 144 × 768 complex points in t_1 and t_2, respectively, and spectral widths of 5000.0 and 12001.2 Hz for F_1 and F_2.

A 3-D $^{13}C/^{15}N$-edited methyl NOESY experiment was recorded on a Varian Inova 600 MHz spectrometer equipped with a pulsed-field gradient triple resonance probe using a 500 ms mixing time and an acquisition time of 50 ms. This is a modified version of the 3-D ^{13}C,^{13}C methyl NOESY experiment of Zwahlen et al. (*36*); in this case ^{13}C and ^{15}N are recorded simultaneously in F_2, allowing for the measurement of both methyl−methyl and methyl−HN NOEs. The experiment used 64 × 32 × 448 complex points in t_1, t_2, and t_3, respectively, and spectral widths of 3000.1, 3000.0 or 1337.3 (for ^{13}C or ^{15}N, respectively), and 9009.9 Hz for F_1, F_2, and F_3. Sixteen scans were acquired for each FID. The ^{1}H, ^{15}N, and ^{13}C carrier frequencies were placed at 5.008, 119.081, and 20.463 ppm, respectively, referenced to external DSS (directly for ^{1}H and indirectly for ^{15}N and ^{13}C chemical shifts) (*37*). For the ^{13}C-edited portion of the methyl NOESY, the size of the F_2 ^{13}C dimension time domain was increased using linear prediction (*38*). After zero-filling three times in each dimension and extraction of the data to retain −0.5 to 2.0 ppm in the acquisition dimension, a 3-D data set of 512 × 512 × 598 real points were obtained. The ^{15}N-edited portion of the methyl NOESY experiment was processed in a similar manner, except that the data were zero-filled twice in each dimension, and the acquisition dimension was extracted to retain 6.5−10.5 ppm to result in a 3-D data set of 256 × 256 × 478 real points.

Aromatic NOE NMR Experiments. All assignment experiments were recorded at 5 °C on a 2.5 mM ^{15}N,^{13}C-labeled drkN SH3 sample in sodium phosphate (50 mM, pH 6), 10% D_2O, and 150 μM DSS. Both of the 2-D (Hβ)Cβ(CγCδ)Hδ and 2-D (Hβ)Cβ(CγCδCϵ)Hϵ experiments (*39*) were recorded on a Varian Inova 800 MHz spectrometer utilizing matrices of 52 × 768 complex points and spectral widths of 6400.0 and 12001.2 Hz for F_1 and F_2. The ^{13}C-^{1}H HSQC (*35*) was recorded on a Varian Inova 800 MHz spectrometer utilizing 64 × 768 complex points in t_1 and t_2, respectively, and spectral widths of 8000.0 and 12001.2 Hz for F_1 and F_2. The 3-D 50 ms $^{13}C/^{15}N$-edited NOESY−HSQC experiment (*40*), recorded on a Varian UNITY Plus 500 MHz spectrometer, utilized a matrix of 128 × 32 × 416 complex points and spectral widths of 5083.9, 3000.0 or 1320.0, and 8000.0 Hz for F_1, F_2, and F_3, respectively. The 3-D HNCα$C\beta$ experiment (*33*), recorded on a Varian UNITY Plus 500 MHz spectrometer, utilized a matrix of 54 × 34 × 512 complex points and spectral widths of 7649.6, 1420.0, and 8000.0 Hz for F_1, F_2, and F_3, respectively.

Aromatic NOE experiments were recorded at 5 °C and utilized a 1.5 mM sample of ^{15}N,^{12}C,^{2}H-labeled drkN SH3 domain with fully ^{15}N,^{13}C,^{1}H-labeled aromatics (Trp, Tyr, Phe, and His) in sodium phosphate (50 mM, pH 6), 10% D_2O, and 200 μM DSS. A 3-D $^{13}C/^{15}N$-edited NOESY−HSQC experiment (*40*) was recorded on a Varian Inova 800 MHz spectrometer with a 600 ms mixing time and an acquisition time of 52 ms, utilizing 128 × 32 × 665 complex points in t_1, t_2, and t_3, respectively, and spectral widths of 8800.9, 5000.0 or 2400.0 (for ^{13}C or ^{15}N, respectively), and 12775.5 Hz for F_1, F_2, and F_3, respectively. Eight scans were acquired for each FID. The ^{1}H, ^{15}N, and ^{13}C carrier frequencies were placed at 4.999, 119.127, and 125.443 ppm, respectively, referenced to external DSS (*37*). For the ^{13}C-edited portion of the NOESY−HSQC, the size of the time domain of the F_2 ^{13}C dimension was doubled using forward−backward linear prediction (*38*). After zero-filling twice in each dimension and extraction of the data to retain 6.5−8.6 ppm in the acquisition dimension, this 3-D data set contained 512 × 256 × 351 real points. The ^{15}N-edited portion of the NOESY−HQSC experiment was processed similarly, except the data were extracted in the acquisition dimension to retain 6.5−10.5 ppm, resulting in a 3-D data set of 512 × 256 × 667 real points.

The 3-D $^{13}C/^{15}N$-edited aromatic NOESY experiment is a modified version of the experiment described by Zwahlen et al. (*36*), except that pulses select the aromatic region rather than that of methyl carbon, and ^{13}C and ^{15}N are recorded simultaneously in F_2, permitting measurement of both side chain aromatic−aromatic and aromatic−HN NOEs. The pulse sequence is available upon request from the lab of Dr. Lewis Kay (contact Ranjith Muhandiram, ranjith@pound.med.utoronto.ca). The experiment was recorded on a

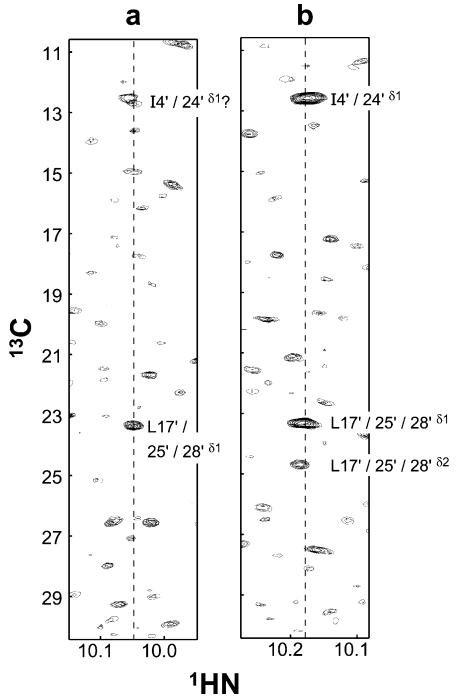

FIGURE 1: Strips of the ^{15}N-edited portion of the methyl NOESY spectrum taken at the ^{1}H and ^{15}N chemical shifts of the Trp 36 indole position ϵ1 in the (a) F_{exch} and (b) U_{exch} states of the drkN SH3 domain. Dashed lines are used to clearly delineate the ^{1}H resonance position in each NOE strip. A prime following a residue number denotes an NOE from the U_{exch} state, while an unprimed number indicates an NOE from the F_{exch} state. Superscripts denote the side chain methyl position. A slash (/) between ambiguous NOEs indicates and/or notation and the ? indicates uncertainty as to whether the assigned position is a peak.

Varian Inova 800 MHz spectrometer with an acquisition time of 50 ms and a mixing time of 600 ms. Matrices of 32 × 32 × 636 complex points were recorded with spectral widths of 5000.0, 5000.0 or 2400.0 (for ^{13}C or ^{15}N, respectively), and 12775.5 Hz (F_1, F_2, and F_3, respectively), and 32 scans were acquired for each FID. The ^{1}H, ^{15}N, and ^{13}C carrier frequencies were placed at 4.999, 119.127, and 125.435 ppm respectively, referenced to external DSS (*37*). For the ^{13}C-edited portion of the aromatic NOESY, the size of the F_2 ^{13}C dimension was doubled using forward−backward linear prediction (*38*). The data were zero-filled twice in each dimension, and the acquisition dimension was extracted to retain 6.1−8.8 ppm in a 3-D data set of 128 × 256 × 431 real data points. The ^{15}N-edited portion of the aromatic NOESY−HQSC experiment was processed similarly, except that the data were extracted in the acquisition dimension to retain 6.5−10.5 ppm, resulting in a 3-D data set of 128 × 256 × 638 real points.

RESULTS

Methyl NOE Data. To investigate aliphatic hydrophobic clustering in the unfolded state of the drkN SH3 domain, a 3-D ^{13}C/^{15}N-edited methyl NOESY experiment was recorded on the selectively methyl protonated, highly deuterated protein using a long (500 ms) mixing time. The experiment yielded two 3-D spectra: the first with {$^{13}C_{meth(i)}$ (^{13}C atom i on the δ-methyl group of Ile or Leu), $^{13}C_{meth(j)}$, $^{1}HC_{meth(j)}$}, and the second with {$^{13}C_{meth(i)}$, $^{15}N_{(j)}$, $^{1}HN_{(j)}$} in {F_1, F_2, F_3}, respectively, permitting measurement of methyl−methyl and methyl−HN NOEs, respectively (Figure 1). The (i, $\geq i + 3$) NOEs are listed in Table 1 and summarized in Figure 2. Limited methyl−methyl NOE data were obtained because δ-methyl chemical shifts are heavily overlapped in the unfolded state. It was therefore difficult to distinguish between NOE strips for different residues and impossible to see many of the cross-peaks since they were frequently close to the diagonal (i.e., for interactions between two Ile methyl groups). The situation was further complicated by the presence of intense peaks because of resolution enhancement (sinc wiggles) that obscured many resonances (example not shown). Analysis of methyl−HN data was more successful even though the majority of the NOEs are ambiguous because of peak overlap (see Table 1b). Nevertheless, in many cases ambiguous NOEs are medium- or long-range regardless of the alternatives, as in the interaction of Y37^{HN} with L47$^{\delta2}$ (i, $i + 10$) and/or L28$^{\delta2}$ (i, $i + 11$). Table 1c includes interactions that may be exchange NOEs (where exchange between U_{exch} and F_{exch} states occurs during NOE transfer) or that correspond to resonances in the spectrum that are extremely weak. For these and the ambiguous NOEs, the uncertainty cannot be resolved because of the absence of symmetry-related peaks in the methyl−HN NOE experiment.

Table 1: NOEs (i, $\geq i + 3$) Involving Methyl Side Chains Observed in the U_{exch} State of the drkN SH3 Domain (Mixing Time 500 ms)[a]

a. Unambiguous methyl−HN and methyl−methyl NOEs

atom 1	atom 2	range
D14	L17$^{\delta}$	3
L17$^{\delta}$	R20	3
A13	L17$^{\delta}$	4
L17$^{\delta}$	T22	5
S18	I24$^{\delta}$	6
L17	I24$^{\delta}$	7
I24$^{\delta}$	E31	7

b. Ambiguous methyl−HN and methyl−methyl NOEs

atom 1	atom 2	range	atom 1	atom 2	range
T22	I24/4$^{\delta}$	2/18	I24	L28/47$^{\delta1}$	4/23
N29$^{\delta21}$	I27/53$^{\delta1}$	2/24	Q23	L28/47$^{\delta1}$	5/24
N29	I27/4$^{\delta}$	2/25	N35$^{\delta21}$	L28/25/47$^{\delta1}$	7/10/12
M30	L28/47$^{\delta1}$	2/17	W36$^{\epsilon1}$	L28/25/17$^{\delta1}$	8/11/19
M30	L28/25/47$^{\delta2}$	2/5/17	W36$^{\epsilon1}$	L28/25/17$^{\delta2}$	8/11/19
N51$^{\delta21}$	I53/48$^{\delta}$	2/3	Y37	L47/28$^{\delta2}$	10/11
N51$^{\delta22}$	I53/48$^{\delta}$	2/3	W36$^{\epsilon1}$	I24/4$^{\delta}$	12/32
M30	I27/4$^{\delta}$	3/26	E40	I27/4$^{\delta}$	13/36
R20	L17/25/28$^{\delta2}$	3/5/8	L41	I27/24/4$^{\delta}$	14/17/37

c. Extremely weak or possible exchange NOEs involving methyl−HN and methyl−methyl contacts

atom 1	atom 2	range
F19	I24$^{\delta}$	5
L17$^{\delta2}$	Q23	6
L47$^{\delta1}$	I53$^{\delta1}$	6
I27$^{\delta}$	L41$^{\delta2}$	14
I4$^{\delta}$	L28$^{\delta2}$	24
I24$^{\delta}$	N51	27
D8	I48$^{\delta}$	40
H7	I48$^{\delta}$	41

[a] NOEs are sorted in ascending order according to the range of their correlation and then according to the residue number. Superscripts refer to the side chain position of the given atom; atoms without superscripts refer to backbone amides. In cases of ambiguous NOEs, the superscript is the same for all options; therefore, the superscript is only listed once. A slash (/) between ambiguous NOEs indicates and/or notation.

Aromatic NOE Data. To further investigate hydrophobic clustering, particularly around aromatic rings, two sets of 3-D NMR NOESY experiments were recorded on the selectively aromatic protonated, highly deuterated drkN SH3

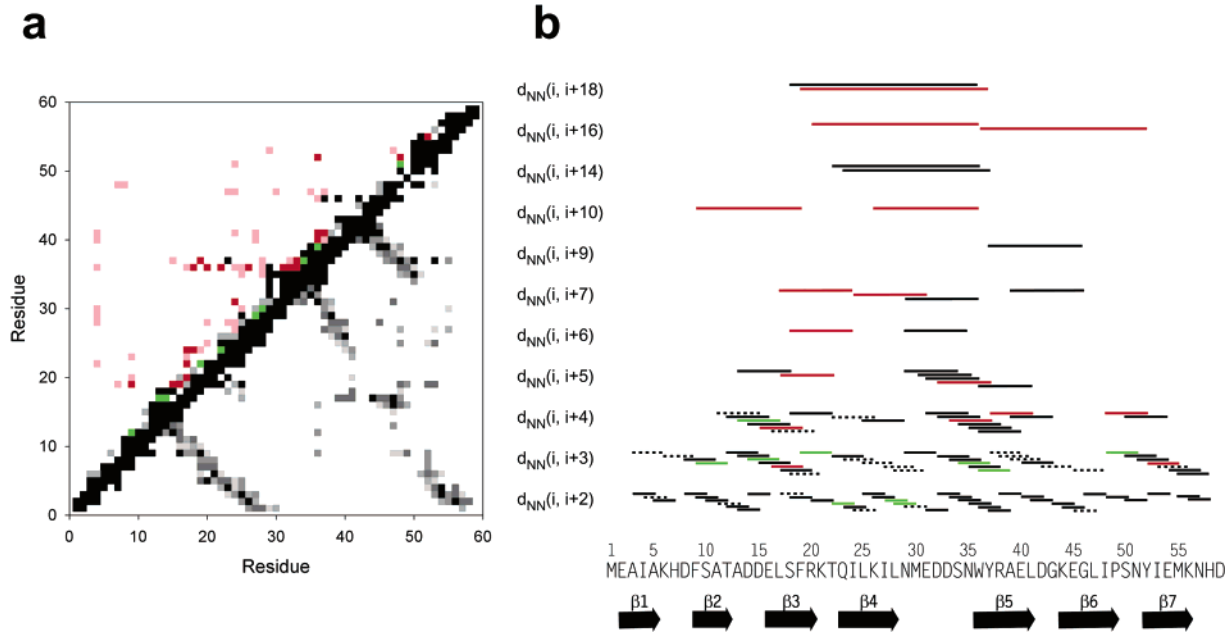

FIGURE 2: Summary of all NOEs observed for the U_{exch} state. (a) Contact map comparing the U_{exch} state NOEs (above the diagonal) to average heavy atom distances (<5.0 Å) per residue in the folded structure of the drkN SH3 domain (below the diagonal). Above the diagonal, black and gray squares denote unambiguous and ambiguous HN−HN NOEs, respectively (taken from Table 1 in Crowhurst et al. (*26*)), and red and pink squares represent unambiguous and ambiguous NOEs involving hydrophobic side chains for the U_{exch} state, respectively. In cases where HN−HN NOEs between two residues in the U_{exch} state are seen in addition to interactions involving hydrophobic side chains, the square is green. The intensities of the squares in the folded state map are scaled by interresidue distances (darker is closer). (b) Solid and broken black lines represent unambiguous and ambiguous U_{exch} state HN−HN NOEs, respectively (*26*), and red lines represent unambiguous NOEs involving hydrophobic side chains. In cases where HN−HN NOEs between two residues are seen in addition to interactions involving hydrophobic side chains, the line is green. The sequence of the drkN SH3 domain and the secondary structure present in the folded state (arrows representing β-strands) are shown at the bottom of the diagram.

domain, with long (600 ms) mixing times. Since the labeling protocol utilized whole aromatic amino acids as precursors, it should also be noted that NOEs involving α and β positions of these residues were recorded in addition to NOEs involving the ring portion of the side chains. The $^{13}C/^{15}N$-edited aromatic NOESY spectra (described in Experimental Procedures) have $\{^{13}C_{aro(i)}$ (^{13}C atom i on an aromatic side chain), $^{13}C_{aro(j)}$, $^{1}HC_{aro(j)}\}$ or $\{^{13}C_{aro(i)}$, $^{15}N_{(j)}$, $^{1}HN_{(j)}\}$ in $\{F_1, F_2, F_3\}$, respectively, permitting measurement of aromatic−aromatic and aromatic−HN NOEs (Figure 3). To combat similar ambiguity problems as those seen in analyzing the methyl NOE data due to the absence of symmetry-related peaks in this aromatic NOESY spectra, a standard 3-D $^{13}C/^{15}N$-edited NOESY−HSQC experiment (*40*) was also recorded, where the ^{13}C-edited spectrum has $\{^{1}H_{(i)}$ (aromatic or HN), $^{13}C_{aro(j)}$, $^{1}HC_{aro(j)}\}$, and the ^{15}N-edited spectrum has $\{^{1}H_{(i)}$ (aromatic or HN), $^{15}N_{(j)}$, $^{1}HN_{(j)}\}$ in $\{F_1, F_2, F_3\}$. Scripts were employed to easily compare NOE data from these two sets of experiments.

In light of previous difficulties in characterizing long-range NOEs for the unfolded state of the drkN SH3 domain (*26*), extreme caution was exercised in the analysis of all data discussed here. In many cases diagonal peaks are very intense, resulting in large resolution enhancement artifacts (sinc wiggles) on all sides. Care was taken to distinguish between these and real peaks; assignments were retained only if symmetry-related peaks or their equivalent could also be observed. Many of the long-range NOEs involving aromatic groups have very weak peaks (i.e., see Figure 3b). In some cases (as in the Tyr 37^{α} to Phe 19^{δ} NOE, Figure 3c), the peak was clearly not a sinc wiggle and could also be assigned unambiguously. Most frequently, assignments were verified by observing corresponding peaks in the second 3-D experiment. In the example of the Arg 20^{HN} to Trp $36^{\zeta 2}$ NOE, the peak seen in the ^{15}N-edited portion of the aromatic NOESY spectrum in Figure 3b could also be observed in the ^{15}N-edited portion of the NOESY−HSQC spectrum. This type of verification is quite powerful since the assignment is independently confirmed by a separate NOESY experiment.

Table 2 and Figure 2 summarize all NOEs involving aromatic side chains of the U_{exch} state of the drkN SH3 domain (except for the three involving the Trp $36^{\epsilon 1}$ interactions to methyl side chains, which are listed in Table 1). For the sake of complete reporting on NOEs of side chain aromatics, Table 2 includes some previously reported HN NOEs to Trp $36^{\epsilon 1}$ (*26*). The quality of the data were far superior to that seen in the methyl−NOE experiments (Figure 3 as compared to Figure 1), primarily because of excellent overall dispersion of the aromatic peaks for both folded and unfolded states. This, combined with the two sets of 3-D NOESY experiments, resulted in a much longer list of unambiguous NOEs with no ambiguous peaks. However, Table 2b lists weak and possible exchange NOEs, which are as defined above for the methyl NOE data. Overall, the significant numbers of medium- and long-range interactions observed in these experiments strongly support the utility of selective protonation in a deuterated background and long NOE mixing times. Specialized NMR experiments allowing for needed resolution and unambiguous assignment of the NOEs were also critical.

NOE Interpretation. The observation of an NOE is taken to imply the presence of conformations with close contacts between these sites within the U_{exch} state ensemble. We have not interpreted NOE intensities or peak volumes in either a

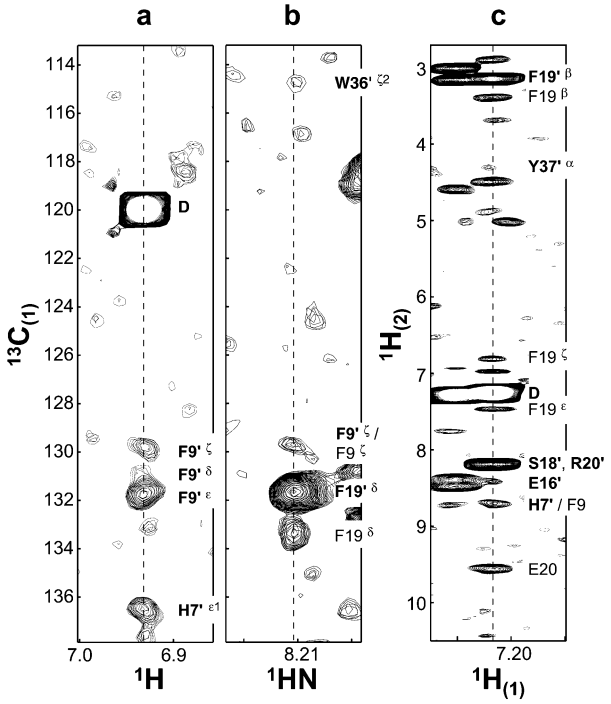

FIGURE 3: Aromatic NOE data for the U_{exch} state of the drkN SH3 domain. (a) Strip from the ^{13}C-edited portion of the aromatic NOESY spectrum taken at the ^{1}H and ^{13}C chemical shifts for His $7^{\delta 2}$ in the unfolded state. (b) Strip from the ^{15}N-edited portion of the aromatic NOESY spectrum taken at the ^{1}H and ^{15}N chemical shifts of Arg 20^{HN} in the unfolded state. (c) Strip from the ^{13}C-edited portion of the NOESY−HSQC experiment taken at the ^{1}H and ^{13}C chemical shifts of Phe 19^{δ} in the unfolded state. Dashed lines are used to clearly delineate the position of the ^{1}H resonance in each NOE strip. A prime following a boldfaced residue number denotes an NOE from the U_{exch} state, while an unprimed number indicates an NOE from the F_{exch} state (exchange NOE). D represents the diagonal peak. Superscripts denote the side chain aromatic position, while no superscript denotes the backbone amide position. A slash (/) between ambiguous NOEs indicates and/or notation; residue labels separated by commas indicate unambiguous NOEs to all listed residues.

quantitative or qualitative manner to derive distance restraints within the U_{exch} state. Differential relaxation within a disordered state due to complex dynamic behavior affects the NMR intensities, particularly with the long mixing times that have been employed in these experiments. In addition, many peaks are overlapped in the spectra; some are heavily overlapped. The peak volume or intensity cannot be determined accurately or consistently for overlapped peaks. Therefore, we assume only an upper distance bound of 10 Å for NOEs observed between any two protons in the U_{exch} state, as determined previously by Mok et al. (*25*) for the F_{exch} state. No structural calculations using this distance bound are described in this work, but the 10 Å limit has been used to determine the consistency of observed NOEs with selected structures of previously calculated conformer pools.

DISCUSSION

Hydrophobic Clustering. Almost all medium- or long-range NOEs listed in Tables 1 and 2 involve methyl or aromatic side chains interacting with other hydrophobic groups or backbone amides of, or adjacent in sequence to, a hydrophobic residue. There are several contacts specifically between aromatic side chains supporting previous near-UV circular dichroism data that implied the presence of residual tertiary contacts involving aromatics (*17*). A majority of the medium- and long-range ambiguous and unambiguous NOEs are non-native, defined as >10 Å separation in the folded state structure (the structure of the folded drkN SH3 domain is described in Bezsonova, I. et al., manuscript in preparation). Few of these NOEs point to any specific contacts between residues in the binding site (which includes primarily aromatic residues and one proline), although the site may still be partially formed because of the general hydrophobic clustering within the U_{exch} state. Partial formation of the binding site in the unfolded state could help explain the fly casting mechanism with which Shoemaker et al. (*41*) propose that unfolded proteins bind their target more rapidly than the folded state since the capture radius of the binding site is larger in a disordered state.

Tryptophan Burial. It has previously been determined that the Trp 36 indole is more buried in the unfolded than the folded state; stopped-flow fluorescence experiments, hydrogen exchange, and near-UV circular dichroism experiments have all provided evidence to support this (*17*, *25*). The HN−methyl NOE strips of Trp $36^{\epsilon 1}$ illustrate another clear difference in the environment surrounding the indole of the folded versus the unfolded states (Figure 1). Note that both assigned peaks for the F_{exch} state (Figure 1a) are exchange NOEs. In other words, the $\epsilon 1$ position of the Trp 36 indole in the folded state has no NOE interactions with methyl-containing groups in the hydrophobic core, which is not surprising since the indole lies on the surface of the folded

Table 2: NOEs ($i, \geq i + 3$) Involving Aromatic Side Chains Observed in the U_{exch} State of the drkN SH3 Domain (Mixing Time 600 ms)[a]

a. Unambiguous aromatic−HN and aromatic−aromatic NOEs

atom 1	atom 2	range	atom 1	atom 2	range
$F9^{\zeta}$	T12	3	S33	$Y37^{\epsilon}$	4
E16	$F19^{\delta}$	3	$W36^{\epsilon 1}$	E40 *	4
$F19^{\delta}$	T22	3	$Y37^{\epsilon}$	L41	4
D33	$W36^{\delta 1}$	3	I48	$Y52^{\epsilon}$	4
D33	$W36^{\epsilon 1}$*	3	E31	$W36^{\epsilon 1}$*	5
S34	$Y37^{\delta}$	3	D32	$Y37^{\epsilon}$	5
$W36^{\epsilon 1}$	A39	3	$W36^{\epsilon 1}$	L4*	5
$W36^{\epsilon 1}$	A39*	3	$F9^{\zeta}$	F19	10
$W36^{\epsilon 3}$	A39	3	K26	$W36^{\zeta 2}$	10
$W36^{\zeta 3}$	A39	3	T22	$W36^{e1}$*	14
$Y52^{\delta}$	M55	3	R20	$W36^{\zeta 2}$	16
$Y52^{\epsilon}$	M55	3	$W36^{\epsilon 3}$	$Y52^{\delta}$	16
D15	$F19^{\delta}$	4	S18	$W36^{\epsilon 1}$*	18
D32	$W36^{\epsilon 1}$*	4	$F19^{\delta}$	$Y37^{\alpha}$	18

b. Extremely weak or possible exchange NOEs involving aromatic−HN and aromatic−aromatic contacts

atom 1	atom 2	range
$Y37^{\delta}$	E40	3
$W36^{\epsilon 3}$	E40	4
D32	$Y37^{\delta}$	5
$W36^{\zeta 3}$	G46	10
$F9^{\zeta}$	R20	11
H7	$F19^{\delta}$	12
$F9^{\zeta}$	Q23	14
D15	$Y37^{\delta}$	22

[a] NOEs are sorted in ascending order according to the range of their correlation and then according to the residue number. Superscripts refer to the side chain position of the given atom; atoms without superscripts refer to backbone amides. An asterisk (*) indicates an NOE previously reported (*26*).

state structure. This is in stark contrast to the three clear peaks in the NOE strip of the U_{exch} state indole, corresponding to at least three NOEs to hydrophobic methyl-containing groups with minimum ranges of (i, $i + 8$) and (i, $i + 12$). The data therefore support previous evidence that Trp 36 is buried in the U_{exch} state ensemble and additionally suggest that the burial is a result of non-native hydrophobic clustering organized by the indole.

In assessing the NOE data as a whole, it is apparent that Trp 36 is likely to be at the center of the hydrophobic clustering in the unfolded state. More than half of all reported NOEs involving the aromatic side chains (Tables 1 and 2, Figure 2) include this indole. The results agree with the research of Klein-Seetharaman et al. (*2*), demonstrating that hydrophobic residues such as tryptophan organize hydrophobic collapse in disordered states. The data also support suggestions that these residues may be partially exposed to solvent in the folded state for functional purposes (Trp 36 is located in the binding site in the folded state of the drkN SH3 domain) but might be buried to facilitate proper folding or to prevent aggregation during folding.

Non-Native Interactions Involving Trp 36 and Tyr 37. Of the long-range NOEs in the U_{exch} state involving Trp 36 and Tyr 37, a number correspond to non-native interactions with residues 18−26, which are located in strand β3 and the diverging turn in the folded state. The computer algorithm AGADIR (*19*, *42*) predicts that residues 16−28 have a high propensity for helical structure. It is therefore interesting that residues Phe 19 and Gln 23, which are in the i and $i + 4$ positions with respect to each other, both make contacts with Tyr 37; note that the Tyr 37^{HN} to Gln $23^{\epsilon 2}$ interaction was reported previously (*26*). The data are consistent with two residues that lie on the same face of an α-helical structure in the unfolded state in close proximity to the tyrosine. This is further supported by interactions between the Trp 36 indole and the backbone amides of Ser 18, Arg 20, Thr 22, and Lys 26; the indole interacts with residues 18, 22, and 26, likely representing the same face of the helix (a different face than the one with which Tyr 37 interacts) since they occupy the i, $i + 4$, and $i + 8$ positions relative to each other. Previous experiments analyzing mutants of Thr 22 indicated that mutations increasing the folding rate and stability of the drkN SH3 domain (such as T22G) were predicted by AGADIR to have a much lower helical content (*19*). Conversely, when this α-helical propensity was stabilized by mutations at the 22 position (such as T22K or T22L), the folded state was destabilized, and the unfolded state was more populated. In the wild type, this is suggestive of a significantly populated conformation or subset of conformations in the unfolded state ensemble in which the aromatic groups Trp 36 and Tyr 37 help stabilize non-native helical structure between residues 16−28. This non-native interaction provides another explanation, in addition to hydrophobic clustering, for the greater burial of the Trp 36 indole in the U_{exch} state than in the folded state (*17*, *25*, *43*).

Structural Trends from NOE Data. Figure 2 illustrates differences in the types of residual structure in the U_{exch} state probed by the HN−HN NOE versus the hydrophobic (methyl and aromatic) NOE data. The most striking difference in comparing the three sets of data is that the HN−HN NOEs are predominantly nativelike short- and medium-range interactions, while the majority of hydrophobic contacts (red lines in Figure 2b representing interactions between residues that do not also have HN−HN contacts) are medium- and long-range, and many are non-native. The short- and medium-range HN−HN NOEs cluster in areas that correspond to loop regions in the folded state structure, particularly around the n-src and RT loops. Longer-range nativelike HN−HN interactions are observed between residues corresponding to the central β-sheet, particularly between the β5 and β6 strands in the folded state. In contrast, the majority of contacts involving hydrophobic groups are longer-range, and taken together cannot be clearly associated with nativelike secondary structure. The only commonality among all three sets of NOE data is the large proportion of NOEs that involve Trp 36.

The NOE data have been compared to some possible unfolded state structures, generated by either TRADES (trajectory directed ensemble sampling (*44*)), as previously described (*45*), or molecular dynamics unfolding simulations of the drkN SH3 domain at high temperatures (Philippopoulos, M., Forman-Kay, J. D., and Pomès, R., manuscript in preparation). Two selected structures from these calculations are shown in Figure 4 to aid in visualizing conformers consistent with the observed NOEs. Nativelike secondary structure observed from the HN−HN NOE data and the hydrophobic clustering seen in the methyl and aromatic NOE experiments (a large portion of which is non-native) appear to segregate in separate conformers within the unfolded state ensemble, although one or more of the loops or turns are possibly well-formed in all conformers. There is a general correlation between maintenance of secondary structure, degree of compactness, and the degree of Trp 36 exposure; maintenance of secondary structure is frequently coupled to a compact overall structure but results in an exposed Trp 36 indole (see Figure 4c). Conversely, many of the unfolded structures with greater burial of the indole than in the folded state contain a compact cluster of residues organized around the Trp 36 but with no regular secondary structure and with a larger overall R_g because of extended N- and C-terminal regions (i.e., see Figure 4b). In particular, the compact structure shown in Figure 4b contains a large cluster of methyl and aromatic residues including Leu 17, Ile 24, Leu 25, Ile 27, Leu 28, Trp 36, Tyr 37, and Leu 41, consistent with nine long-range NOEs measured in the U_{exch} state (<10 Å separation). In contrast, hydrophobic groups are dispersed in the conformer in Figure 4c (side chains not shown) but have many short-, medium-, and long-range nativelike U_{exch} state NOEs within areas corresponding to the n-src loop, diverging turn, and between residues corresponding to the β4, β5, and β6 strands in the folded state. (These contacts are indicated on the C^{α} trace in Figure 4c.) Many nativelike NOEs corresponding to the RT loop region are also consistent with this conformer, although a tight loop is not present in this conformer. Thus, while the HN−HN NOEs highlight preservation of nativelike secondary structure in the central β-sheet, the hydrophobic NOE data demonstrate the non-native interaction between Trp 36/Tyr 37 and the β3/diverging turn region and many medium- and long-range contacts. These latter data are suggestive of conformations with less specific clustering in the central β-sheet region, possibly mediated by long-range hydrophobic contacts.

The conformers shown in Figure 4 are merely two salient examples of the many conformers that fit some portion of

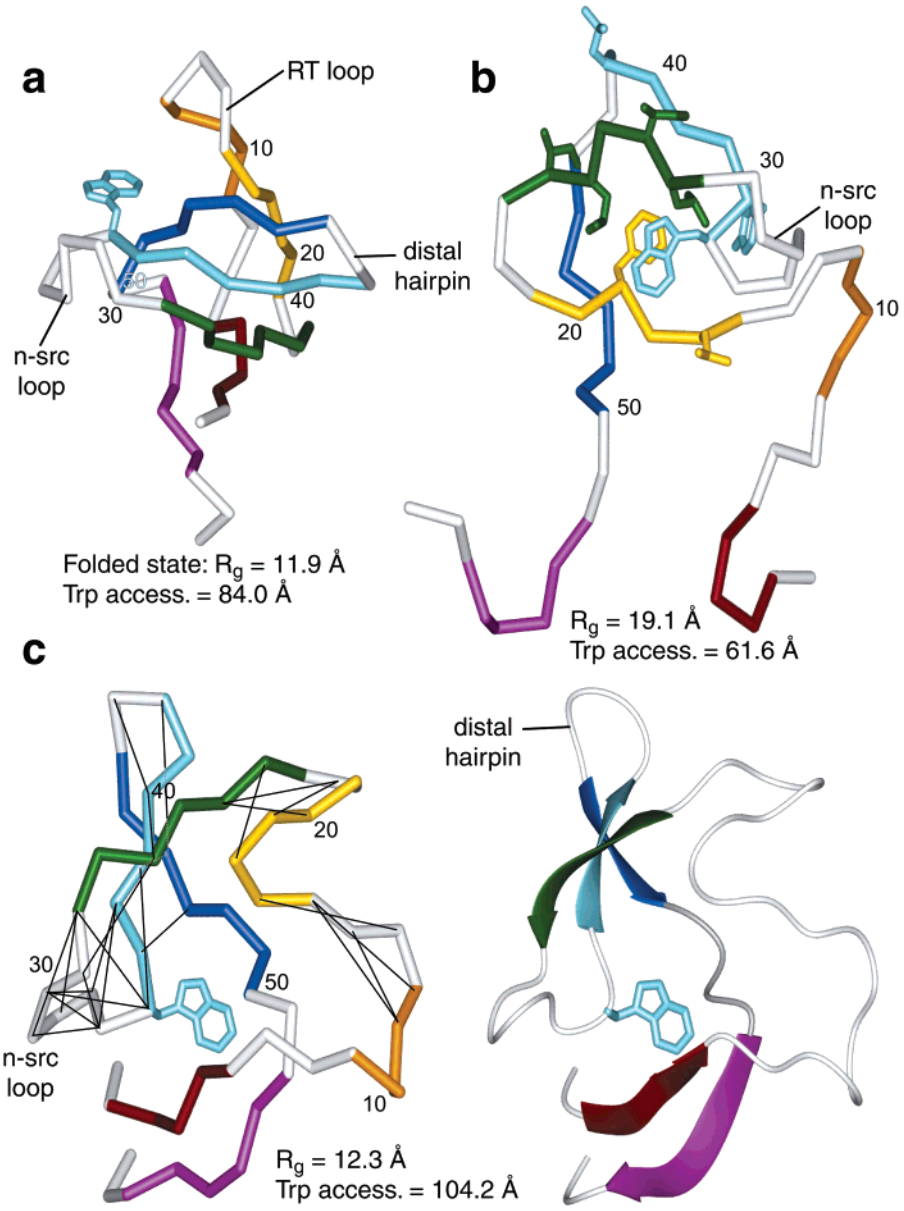

FIGURE 4: Structures of the folded state and illustrative unfolded state conformers consistent with the NOE data. The residues corresponding to the seven β-strands of the folded state are as follows: β1, red; β2, orange; β3, yellow; β4, green; β5, light blue; β6, dark blue; and β7, purple. Some loops and turns of the folded state are labeled for clarity. The radius of gyration (R_g) and solvent accessibility of the Trp 36 indole are provided below each structure, and the Trp 36 side chain is added in panels a and c as a visual reference. (a) The folded state structure (Bezsonova et al., manuscript in preparation). (b) A possible U_{exch} state conformer illustrating non-native hydrophobic clustering generated using TRADES (*44*). Side chains involved in this hydrophobic cluster that are also consistent with experimentally measured U_{exch} state NOEs (<10 Å distance between residues) are included in the figure. (c) A possible U_{exch} state conformer illustrating a residual nativelike β-sheet structure taken from a high-temperature unfolding molecular dynamics trajectory (Philippopoulos, M. et al., manuscript in preparation). The C^{α} trace on the left shows lines corresponding to nativelike NOEs measured in the U_{exch} state that are satisfied in this conformation (<10 Å distance between residues). A ribbon diagram of the same conformer is shown on the right to indicate the locations of residual β-structure. The figure was generated using Molmol v2K.2 (*47*) and rendered by POV-Ray for Windows v3.1.

the data; they have been chosen to represent the wide variety of conformers that must be present within the U_{exch} ensemble to account for all of the observed NOEs. We are currently working with ENSEMBLE, our software program developed to calculate ensembles of structures representing the unfolded state based on experimental data (*45*), to generate a new ensemble for the U_{exch} state based on this new NOE data as well as other experimental results reported for the drkN SH3 domain. As is evident from the significance of the non-native NOEs observed here, the library of possible conformers must be expanded to include structures with more non-native interactions and secondary structural elements than utilized in previous ENSEMBLE calculations (*45*).

The results of these NOE experiments correspond closely to previously reported data, clarifying structural characteristics of the U_{exch} state of the drkN SH3 domain. The observed nativelike NOEs clustered in regions corresponding to the RT and n-src loops as well as the central β-sheet in the folded state provide further support for residual nativelike interactions in these regions being cooperatively disrupted in the U_{exch} state upon denaturation based on chemical shift changes (*17*). The non-native hydrophobic clustering in the

U_{exch} state evidenced by these NOE experiments is in agreement with near-UV circular dichroism spectra implying tertiary interactions involving all aromatic groups, especially for the Trp 36 peak that is as intense in the unfolded as in the folded state (*17*). Side chain relaxation data also exhibit restriction of aromatic ring motions that are consistent with hydrophobic clustering in the unfolded state (*43*). Stopped-flow fluorescence and hydrogen exchange experiments provide strong additional support that the Trp 36 indole is more buried on average in the U_{exch} than the F_{exch} state (*17*, *25*). Finally, J_{HNHA} coupling experiments demonstrating non-native α-helical propensity for residues 16−20 in the U_{exch} state (*12*) correspond to the current NOE data indicating non-native interactions involving Trp 36/Tyr 37 and residues in the β3 strand/diverging turn region, which may stabilize an α-helix.

In summary, analysis of all three NOE experiments highlights a wider range of conformers within the unfolded state ensemble than data from only the HN−HN NOEs. The observed conformers include highly nativelike compact structures maintaining secondary structure as well as less compact species containing regions of long-range hydrophobic contacts. These former conformers are consistent with a hierarchic condensation model of folding, while the latter conformers are consistent with conformations that have been proposed to form at the initiation of the hydrophobic collapse model of folding. While the results described here are not kinetic data, they are consistent with the folding funnel view of protein folding (*46*), in which the drkN SH3 domain may fold along either of these two pathways or proceed via a route that embraces a combination of these two extremes. In addition, the significant interactions including secondary structure and long-range hydrophobic contacts help to explain the stability of the unfolded state of the drkN SH3 domain, which is almost 50% populated at 5 °C in its equilibrium with the folded state under nondenaturing conditions.

ACKNOWLEDGMENT

The authors sincerely thank Drs. Lewis Kay and Ranjith Muhandiram for development of the aromatic NOESY experiment and for NMR assistance with all experiments. We are grateful as well to Drs. Natalie Goto, Ronald Venters, and Geoffrey Mueller for technical advice during preparation of the selectively labeled samples and to Dr. Wing-Yiu Choy for many helpful discussions throughout the processes of data analysis and manuscript preparation.

REFERENCES

1. Grantcharova, V., Alm, E. J., Baker, D., and Horwich, A. L. (2001) *Curr. Opin. Struct. Biol. 11*, 70−82.
2. Klein-Seetharaman, J., Oikawa, M., Grimshaw, S. B., Wirmer, J., Duchardt, E., Ueda, T., Imoto, T., Smith, L. J., Dobson, C. M., and Schwalbe, H. (2002) *Science 295*, 1719−1722.
3. Shortle, D. (1996) *FASEB J. 10*, 27−34.
4. Dyson, H. J., and Wright, P. E. (1998) *Nat. Struct. Biol. 5*, 499−503.
5. Yao, J., Chung, J., Eliezer, D., Wright, P. E., and Dyson, H. J. (2001) *Biochemistry 40*, 3561−3571.
6. Hodsdon, M. E., and Frieden, C. (2001) *Biochemistry 40*, 732−742.
7. Mok, Y.-K., Alonso, L. G., Lima, L. M. T. R., Bycroft, M., and de Prat-Gay, G. (2000) *Protein Sci. 9*, 799−811.
8. Griffiths-Jones, S. R., and Searle, M. S. (2000) *J. Am. Chem. Soc. 122*, 8350−8356.
9. Chakraborty, S., and Peng, Z. (2000) *J. Mol. Biol. 298*, 1−6.
10. Fong, S., Bycroft, M., Clarke, J., and Freund, S. M. (1998) *J. Mol. Biol. 278*, 417−429.
11. Zhang, O., Kay, L. E., Shortle, D., and Forman-Kay, J. D. (1997) *J. Mol. Biol. 272*, 9−20.
12. Zhang, O., and Forman-Kay, J. D. (1997) *Biochemistry 36*, 3959−3970.
13. Gardner, K. H., and Kay, L. E. (1998) *Annu. Rev. Biophys. Biomol. Struct. 27*, 357−406.
14. Gardner, K. H., and Kay, L. E. (1997) *J. Am. Chem. Soc. 119*, 7599−7600.
15. Mal, T. K., Matthews, S. J., Kovacs, H., Campbell, I. D., and Boyd, J. (1998) *J. Biomol. NMR 12*, 259−276.
16. Kelly, M. J. S., Krieger, C., Ball, L. J., Yu, Y., Richter, G., Schieder, P., Bacher, A., and Oschkinat, H. (1999) *J. Biomol. NMR 14*, 79−83.
17. Crowhurst, K. A., Tollinger, M., and Forman-Kay, J. D. (2002) *J. Mol. Biol. 322*, 163−178.
18. Farrow, N. A., Zhang, O., Forman-Kay, J. D., and Kay, L. E. (1995) *Biochemistry 34*, 868−878.
19. Mok, Y. K., Elisseeva, E. L., Davidson, A. R., and Forman-Kay, J. D. (2001) *J. Mol. Biol. 307*, 913−928.
20. Tollinger, M., Skrynnikov, N. R., Mulder, F. A. A., Forman-Kay, J. D., and Kay, L. E. (2001) *J. Am. Chem. Soc. 123*, 11341−11352.
21. Tollinger, M., Forman-Kay, J. D., and Kay, L. E. (2002) *J. Am. Chem. Soc. 124*, 5714−5717.
22. Zhang, O., and Forman-Kay, J. D. (1995) *Biochemistry 34*, 6784−6794.
23. Zhang, O., Forman-Kay, J. D., Shortle, D., and Kay, L. E. (1997) *J. Biomol. NMR 9*, 181−200.
24. Choy, W.-Y., Mulder, F. A. A., Crowhurst, K. A., Muhandiram, D. R., Millett, I. S., Doniach, S., Forman-Kay, J. D., and Kay, L. E. (2002) *J. Mol. Biol. 316*, 101−112.
25. Mok, Y.-K., Kay, C. M., Kay, L. E., and Forman-Kay, J. (1999) *J. Mol. Biol. 289*, 619−638.
26. Crowhurst, K. A., Choy, W.-Y., Mok, Y.-K., and Forman-Kay, J. D. (2003) *J. Mol. Biol. 329*, 185−187.
27. Goto, N. K., Gardner, K. H., Mueller, G. A., Willis, R. C., and Kay, L. E. (1999) *J. Biomol. NMR 13*, 369−374.
28. Delaglio, F., Grzesiek, S., Vuister, G. W., Zhu, G., Pfeifer, J., and Bax, A. (1995) *J. Biomol. NMR 6*, 277−293.
29. http://spin.niddk.nih.gov/bax/software/NMRPipe/info.html.
30. Johnson, B. A., and Blevins, R. A. (1994) *J. Biomol. NMR 4*, 603−614.
31. http://www.nmrview.com.
32. Zhang, O., Kay, L. E., Olivier, J. P., and Forman-Kay, J. D. (1994) *J. Biomol. NMR 4*, 845−858.
33. Muhandiram, D. R., and Kay, L. E. (1994) *J. Magn. Reson. Ser. B 103*, 203−216.
34. Grzesiek, S., Anglister, J., and Bax, A. (1993) *J. Magn. Reson. Ser. B 101*, 114−119.
35. Santoro, J., and King, G. C. (1992) *J. Magn. Reson. 97*, 202−207.
36. Zwahlen, C., Gardner, K. H., Sarma, S. P., Horita, D. A., Byrd, R. A., and Kay, L. E. (1998) *J. Am. Chem. Soc. 120*, 7617−7625.
37. Wishart, D. S., Bigam, C. G., Yao, J., Abildgaard, F., Dyson, H. J., Oldfield, E., Markley, J. L., and Sykes, B. D. (1995) *J. Biomol. NMR 6*, 135−140.
38. Zhu, G., and Bax, A. (1992) *J. Magn. Reson. 98*, 192−199.
39. Yamazaki, T., Forman-Kay, J. D., and Kay, L. E. (1993) *J. Am. Chem. Soc. 115*, 11054−11055.
40. Pascal, S. M., Muhandiram, D. R., Yamazaki, T., Forman-Kay, J. D., and Kay, L. E. (1994) *J. Magn. Reson. Ser. B 103*, 197−201.
41. Shoemaker, B. A., Portman, J. J., and Wolynes, P. G. (2000) *Proc. Natl. Acad. Sci. U.S.A. 97*, 8868−8873.
42. Munoz, V., and Serrano, L. (1995) *J. Mol. Biol. 245*, 275−296.
43. Yang, D., Mok, Y.-K., Muhandiram, D. R., Forman-Kay, J. D., and Kay, L. E. (1999) *J. Am. Chem. Soc. 121*, 3555−3556.
44. Feldman, H. J., and Hogue, C. W. V. (2000) *Proteins 39*, 112−131.
45. Choy, W.-Y., and Forman-Kay, J. D. (2001) *J. Mol. Biol. 308*, 1011−1032.
46. Dill, K. A., and Chan, H. S. (1997) *Nat. Struct. Biol. 4*, 10−18.
47. Koradi, R., Billeter, M., and Wüthrich, K. (1996) *J. Mol. Graph. 14*, 51−55 and 29−32.

BI034601P